ORIGINAL ARTICLE

A Novel Way to Overcome Problems Arising in Strain Signal Measurements Leading to a Fatigue Failure Characterisation

T. E. Putra[1*], S. Abdullah[2] and D. Schramm[3]

[1]Department of Mechanical Engineering, Universitas Syiah Kuala, Darussalam 23111, Banda Aceh, Indonesia
Phone: +6282310349465
[2]Department of Mechanical and Materials Engineering, Universiti Kebangsaan Malaysia, 43600 UKM-Bangi, Selangor, Malaysia
[3]Departmental Chair of Mechatronics, Universität Duisburg-Essen, 47057 Duisburg, Germany

ABSTRACT – The aim of this study is to identify the issues that arise when measuring a strain signal in order to characterise fatigue failure. In traditional methods, acquisition of a strain signal is constrained due to the presence of errors, time-consuming process and associated high cost. In this study, a new method for generating strain signals based on computer simulation was proposed. A strain gauge was positioned near the citical area pertaining to an automotive coil spring driven on road surfaces in order to measure strain signals. The strain signals were utilised for the inputs in the simulation. For validation purposes, the actual and simulated strain signals were examined by performing fatigue tests. The actual and simulated urban strain signals, respectively, required 412 and 415 reversals of blocks. For the rural road, the fatigue life was 137 and 139 reversals of blocks, respectively, for the actual and simulated strain signals. These indicated that simulated strain signals were accurately generated, providing a minimum fatigue life deviation, which was lower than 1.5 %. By developing the strain signals of a component through simulation, its integrity and fatigue failure can adequately be determined, thereby, saving the cost associated with operation and maintenance. Thus, the simulation is expected to assist the automotive industries involved with strain signal acquisition.

INTRODUCTION

Fatigue is a kind of failure triggered by different amplitude loadings. In this particular scenario, loads regulated by a component would not be able to attain an adequate level competent enough to trigger failure in a single operation. When loads are consistent and unceasing, they lead to loss of flexibility and as a result of this develop into cracks, and components failure. This failure which occurs gradually, locally, and permanently, is dependent on repeated and vigorous stresses that affect the critical areas, where the stress is lower than the ultimate tensile strength and the static yield strength [1-2].

The presence of residual stresses on a component could affect the component durability. If these residual stresses were retained for a long time, they could increase the likelihood of an occurrence of the fatigue failure of that component. Computer modelling, laboratory experiments and component testing are main engineering activities which complement the durability analysis [3]. The durability of a component can be tested with the help of service loads. For the durability analysis, a good knowledge of the service loads is essential, as they are used for testing components in different engineering applications. Therefore, during the early product development stage, engineers must predict the strain and stress histories for modelling and designing mechanical fatigue [1,4].

Most of the fatigue lives are conventionally predicted utilising a constant amplitude loading (CAL) for obtaining a strain-life or stress-life curve. However, most of the fatigue signals in real applications show various behaviour providing a challenge [5-7]. This process involves three phases, namely signal collection, signal processing and result analysis. Regrettably, a fatigue signal is not easy to be obtained directly, and the acquisitions bear a high cost and consume a lot of time [8-9].

In general, a strain signal measurement technique could be segmented as equipment installation and strain signal measuring stages. As per Motra et al. [10], strain gauge sensors are commonly employed to measure strain signal due to their accuracy, credibility, cost-effectiveness, reliability, and ease of use. Nevertheless, it is often misused, leading to measurement irregularities and uncertainty. Strain gauge produces constant value only in the elastic and plastic region. However, the contact with a test piece is lost, resulting in displaying inaccurate or no value due to inconsistencies involved in the bonding. There are numerous error sources inherent the resistance strain gauge measuring system, such as the transverse sensitivity of the strain gauge, temperature and misalignment.

It needs to be noted that the global veracity of the measuring system is impacted by systematic errors, while precision and accuracy are impacted by random errors. The raw signal's quality relies on the employed measuring model in order to actuate the ambivalence involved with the best value pertaining to the quality that has to be measured. The wired strain

measurement includes inherent constraints and disadvantages in terms of industrial implementation due to specialised effort made to protect and route cables in the harsh environment [11]. Despite strain gauge being weak for strain signal acquisitions, it is still regarded as an important sensor for measuring a strain signal.

In the last two decades, several strain signal measurements have been done to observe a dynamic structural response. The acquired strain signal utilises a strain gauge was used to validate the fatigue data editing (FDE) method for trains on a light railway. In this study, it has analysed a train running on its track at a speed of 80 km/h, a length of 2.4 km, and by considering a sampling frequency of 500 Hz, and found that it produced a total of 103,700 data points. Various levels of noise have been dictated pertaining to the signal damage [12]. Next, different strain signals were captured by Haiba et al. [13] at the automotive lower arm to assess the impact of several evaluation techniques on fatigue life. A speed of 34 km/h was used to drive the vehicle over a virtual pavé track which displayed an insignificant change in the mean of the signals with little low-frequency content.

Ilic [14] also employed strain gauges to amass the applied loads pertaining to automatic transmission systems in order to validate the data decrease method. The vehicle was driven on different kinds of roads with various velocities. It was driven on a 50 km minor road segment with an average speed of 43 km/h for more than 70 minutes. The vehicle was also driven for a distance of 50-km, more than 35 minutes on the highway segment at an average speed of 86 km/h. Moreover, the vehicle was driven on the 72-km winding road segment at an average speed of 72 km/h for more than 60 minutes. Lastly, the vehicle was driven for 20 km at an average speed of 17 km/h for more than 70 minutes on the built-up portion.

A strain gauge was employed by Abdullah et al. [15] to gather a strain signal at an automotive lower arm in order to validate FDE. The car travelled at a speed of 34 km/h in a pavé road generating a total recorded length of 46 seconds. Baek et al. [16] acquired a strain signal at a freight vehicle bogie in order to determine the fatigue life by accounting for the rain flow cycle counting method. The signal was captured when the car travelled at 60 km/h for 25 minutes from the start and brake. The strain signals were measured by Alaoui et al. [17] at a ship structure to assess the impact of loading conditions on the behaviour of short crack as well as for the analysis of fatigue crack life. The conditions of the sea, wind, and waves, subjected the ship to variable loadings. On various road surface profiles, He et al. [18] also acquired strain signals pertaining to an automotive damper spring tower.

Oskoueian and Nuawi [19] used strain gauges to observe the condition of an internal combustion engine block. After strain gauges were installed, the four-cylinder engine ran. In the beginning, the engine was not stable and leads to interrupt in signal measurement. Therefore, to become stable, the engine has to work for a few minutes. Using strain gauges, Aygül et al. [20] gathered the stress gradients, excluding the local notch stress in a bid to hypothesise the strains at certain distances from the weld toe. Measurement of the strain signals was done from static tests carried out before fatigue tests. The acquisitions of elastic strain pertaining to various load levels were employed for determining the hot spot stresses and also for evaluating the finite element models pertaining to numerical investigations.

Lin et al. [21] attached a number of strain gauges at some stress concentration points to monitor the responses of the bridge deck connection during the fatigue and maximum design load tests. Xia et al. [22], Ye et al. [23] and Ye et al. [24] employed more than 100 strain gauges sampled at 25.6 Hz, 51.2 Hz and 10 Hz, respectively, to capture dynamic strain responses pertaining to bridge deck sections from the impacts of highway traffic, railway traffic, monsoon, temperature, and typhoon. The strain signals were constantly gauged over a year.

Kihm and Delaux [25] captured some responses at a probable failure zone of a radiator using strain gauges. Data obtained was carried out at 4,096 samples per second with an outstanding resolution of more than forty points and the highest frequency. To prevent uncertainties which are likely to result in design and structural stress differences, Lei et al. [26] acquired the actual strain signal using a pressuriser. Strain gauges were used to obtain the strain signals used as the fundamental data for pressurising the structural integrity or ageing condition during its operation. Nonetheless, the strains varied concerning location. The pressures reduced from the lower to upper head with the same circumference deformation variation. A strain-based measurement approach proposed by Stoney et al. [11], which made use of wired resistive strain gauges was used to measure the broaching tool. High-speed data acquisition was used to monitor sensor signals. This was done using an analogue input channel of 5 kHz with a frequency of 45 Hz. However, the instrument may still possess some additional sources of noise that could interfere with the signal in the sensors.

Strain signals on a coil spring were also measured by Putra et al. [27] for generating simulated strain signal giving errors less than 10 %. 60-second strain data with 5 % noise were measured by He et al. [28] in order to acquire the strain responses, especially at critical spots with regards to the empirical mode decomposition. Putra et al. [29-30] also collected strain signals for validating FDE based on experimental. Zhang et al. [31] used strain signals to identify the golf swing. The developed algorithm was found to be useful in identifying swing signature of golf players. Nasir et al. [32] collected a strain signal to study the reliability of the decomposition using the Gumbel distribution model. The model was able to identify decomposition signal characteristics. Rahim et al. [33] collected a strain signal under rural road condition for denoising based on discrete wavelet transform. Lately, Silva et al. [8] proposed a methodology for the measurement of strain using an Arduino Uno board. The results were in agreement with the literature and gave satisfactory accuracy.

For getting a strain signal on relevant parameters, a measurement is an infinite set of instrumentations. However, there is anyway a likelihood that the intended outcomes cannot be provided, thus making the acquisition an overall waste of resources and fiscal loss. Errors inherent a measurement arises from uncontrollable and unavoidable variations that tend to change the mean and amplitude stress. The errors, owing to poor measuring apparatuses, and interference of physical processes affects the amplitude cycles and hinders accurate assessment. Consequently, fatigue monitoring of a structure is constrained by the quantity of available practical technique [34].

Due to the limitations of acquiring equipment utilised, the reliability and accuracy of strain signals decrease and are often in question, as the strain magnitudes are often small [10]. Errors would directly impact the attained outcomes, thus driving inappropriate inferences. Possessing accurate, precise strain measurement, through which the stresses can be attained, is one of the most significant estimators of fatigue [9,28,35]. One effort to eliminate the noise in a strain signal is filtering. Fatigue signals are often low-pass filtered to decrease lower amplitudes found in the higher frequency region. Unfortunately, this method almost certainly decreases fatigue damage. This technique levels the high amplitude signals, thereby lowering the loading ranges. When employing a strain signal in carrying out fatigue research studies, experimental expenses and error were found to impede the process. The restraints of strain signal measurement lead to the use of CAL in performing the majority of the fatigue tests.

Because of imprecise measuring apparatuses, errors might exist. Almost all fatigue signals measured in engineering practices contain noise [34]. If there is no elimination of the noise from the signal, vital information is corrupted, and the working state might be distorted [36]. Thus, the signal trends need to be extracted from the noise during signal analysis [37-40]. Besides being error-prone, expensive and time-consuming, strain signal acquisition processes require high levels of skill [1,10,31].

Many techniques are available for obtaining a strain signal, and every approach has its own merits and demerits. Therefore, the current study discusses the prohibitions of strain signal measurements and the efforts involved in solving them. In addition, this work proposes a new method for generating strain signals based on computer simulation with consideration of road surface profiles that may lead to fatigue failure. If this method is deployed, the conventional way of obtaining a strain signal, which consumes a lot of time, incurs high costs and is riddled with errors, can be abandoned.

MATERIALS AND METHODOLOGY

In this paper, automotive frontal coil spring with 1,300 cc capacity was utilised as a case study. A static McPherson strut suspension system was employed that possessed a damping coefficient of 15,564 Ns/m and spring stiffness of 18,639 N/m. For simulation, SAE5160 carbon steel was selected as the material. It is usually employed in numerous automotive companies in order to fabricate coil springs. Its physical properties are illustrated in Table 1.

Table 1. Mechanical properties of the SAE5160 carbon steel [41].

Properties	Value
Ultimate tensile strength, S_u (MPa)	1,584
Material modulus of elasticity, E (GPa)	207
Yield strength (MPa)	1,487
Fatigue strength coefficient, σ'_f (MPa)	2,063
Fatigue strength exponent, b	-0.08
Fatigue ductility exponent, c	-1.05
Fatigue ductility coefficient, ε'_f	9.56
Cyclic strain-hardening exponent	0.05
Cyclic strength coefficient (MPa)	1,940
Poisson ratio	0.27

Measurement of a data was done to get strain signals at the coil spring, which was impacted by road surfaces when a strain gauge was positioned in a critical location within the component. The stress distribution on the coil spring was determined via dynamic analysis. To the bottom of the component, a force of 3,600 N was applied while the upper region was kept fixed. The car weight was considered as 10,600 N, while the weight of the other load and passengers was considered to be 3,800 N. Furthermore, the estimated overall force was then divided by four, as it was assumed that the weight of the car and the passengers would be uniformly distributed on the four coil springs. The magnitude of the load used to carry out the cyclic analyses was from 0 to 3,600 N.

In general, the high-stress location for a component is determined by employing a finite element analysis pertaining to the placing of strain gauge installation. Higher strain amplitude is associated with the strain gauge that is placed on a high-stress location, which can be easily measured with the help of a sensor. The state of the strain gauge while measuring the system is a crucial factor in ensuring the accuracy of a strain signal. To do this, the sensor installation process is thoughtfully and cautiously carried out [42]. During the installation process, a good number of factors are addressed to avoid reading errors. Firstly, users have to ensure the integral surface is flat and free from dirt, in which installation of the strain gauge will be done. To achieve a flat surface, the area is scrubbed with sandpaper [43]. To get accurate readings, one needs to make sure that the strain gauge has been maintained in the surface. Secondly, ample care needs to be taken in order to make sure that for both strain gauge poles, the component is not touched by the copper wires or come in contact with each other to avoid short circuits capable to producing inaccurate readings. Thirdly, the adhesive applied is suitable. Should the adhesive be lesser than what is needed, it could result in strain gauge to wear off. In a similar manner, the excessive adhesive could also weaken the sensitivity of the sensor.

Thereafter, to a data logging device, linking of the strain gauge is done in order to record the strain signals detected by the sensor. Acquiring parameters are setup utilising a software package for aligning the sensor reader. In a previous study, Ilic [14] suggested using a sampling frequency value above 400 Hz for obtaining strain signals. This allows thwarting the loss pertaining to the vital components of the signal. Should the collection rate be greater than 500 Hz, it

becomes important to increase the upper-frequency range value, as it helps to build up high-frequency load cycles as well as smaller amplitudes. In addition to this, assembling the load histories at 500 Hz aids in disclosing and apprehending the damaging load cycles which are usually higher than 50 Hz with a lesser amplitude compared to their endurance limits [13]. Figure 1 provides an example of the installation of a strain gauge. Moreover, the vehicle needs to be driven on both the urban and rural roads by maintaining the speed limits within 30-40 km/h and 20-40 km/h, respectively. The speeds as mentioned above were compared to the average rate of the vehicle that was obtained when the car was driven on both urban and rural roads, respectively.
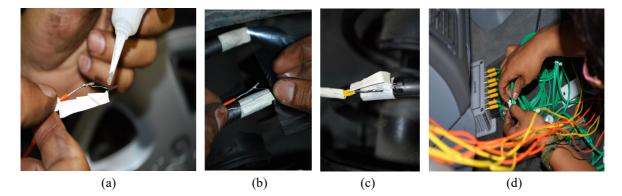

| (a) | (b) | (c) | (d) |

Figure 1. The strain gauge installation: (a) applying the adhesive, (b) placing the strain gauge, (c) installing the strain gauge, and (d) connecting the sensor to the data acquisition.

There are high and low risks associated with product development [44]. From an economic view, industries are seeking solutions to minimise costs eliminate experimental difficulties [45-46]; industries today are dependent on computer simulations for analysing trends prior to investing in real tests. To reduce the pertinent expenditure, a miniature is generated with simulations galloped on it for making sure there is an improvement on the trend and to enable one to proceed with the actual experimentation. This makes it possible to conduct necessary assessments before the development of a system, enhances the need for costly experiments, and can offer support during the various stages of a project.

Lots of associated with the automotive field have been resolved. This could be achieved by simulating the dynamic behaviour pertaining to the structural components that act on the dynamic forces. As per Hooke's law, the displacement x pertaining to an elastic object is regarded to be directly proportional with the applied force P_s as explained below:

$$P_s = kx \tag{1}$$

where k is the spring stiffness. Given that the elastic limit is not exceeded, it is obtained a straight line passing through the origin on plotting a graph of force against the extension. The gradient will produce the spring stiffness. When an experiment is carried out, the spring stiffness is observed to differ, dependent on the objects and materials utilised. The greater the stiffness, the harder the spring, and the softer the spring, the longer the vibration time and a higher mass [47].

The averted mass because of the spring is regarded to be proportional with the needed force in order to expedite the spring system. The associated stiffness with the spring exerts a restoring force required to balance the mass, while dampers rebels any displacement from the equilibrium. The result obtained from frictional effects or viscous is known as damping. If such a force turns out to be proportional with the velocity, the damping force P_d could be linked with the velocity $\dot{x}$ as:

$$P_d = d\dot{x} \tag{2}$$

where d is damping coefficient.

Vibrations are caused by imperfections. Vibration can be defined as any periodic process, in particular the rapid linear motion pertaining to a body with regards to the equilibrium position. This motion causes a change in displacement. Velocity is a vector quantity representing the rate of change in position in tandem with time or speed along with the directional component. It can also be defined as the slope pertaining to the displacement curve. The change in velocity with time is acceleration and can be described as the slope of the velocity curve. Displacement, velocity, and acceleration could also be regarded as vibration or shock dependent on the waveform pertaining to the force function that stimulates acceleration. Whenever an oscillatory force function causes an acceleration, that acceleration is illustrated as a vibrational force. A shock load is basically a force input characterised by a large amplitude and short duration [48].

Vibration could be assessed with regards to its degree of freedom defined as the number of free kinematic variables demonstrating the motion pertaining to a system. Figure 2 shows a mass-spring-damper system that possesses a distinct degree of freedom. It shows the relation amongst the mass, resistance, energy dissipation, and applied force.
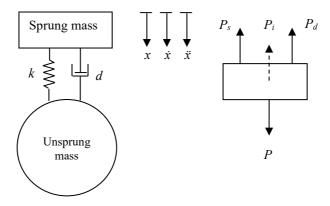
Figure 2. A mass-spring-damper system and its free body diagram.

As per Newton's second law of motion, an object's acceleration relies on two variables: the object mass and the net force that acts on the object. The movement of the mass-spring-damper system is dependent on the applied force. The effects can be defined as a function pertaining to the applied force as well as the mass of different components. The equation pertaining to this system is based on Newton's second law of motion:

$$P_i + P_d + P_s = P \tag{3}$$

where P is the applied force and P_i is the inertial force. An inertial force resists velocity change pertaining to an object, which is equivalent to and in the opposite direction pertaining to an applied force and a resistive force. The inertial force is described as:

$$P_i = m\ddot{x} \tag{4}$$

where m is the mass and $\ddot{x}$ is the acceleration. Submitting Eqs. (1), (2) and (4) into (3), the equation of motion might then be articulated as:

$$m\ddot{x} + d\dot{x} + kx = P \tag{5}$$

All the over dots signify a product of time. This equation shows the performance pertaining to a physical system as well as its motion in terms of time function. The forces associated with damp and spring are equal to the velocity and displacement, respectively, while the inertial force relies on the acceleration. Based on the free-body diagram in Figure 2, the forces of the spring and damp must be proportional to the effect of inertia. According to Eq. (5), some analysts have revised automotive suspension designs that aids in the effectiveness of the suspension system, such as body acceleration controller [47] and vehicle handling stabilisation [49].

Encouraged by the studies on automotive suspension system simulations, Putra et al. [27] carried out a research work by employing the equation of motion as the primary formula to create a mathematical function to get strain signals in a coil spring. Eq. (5) demonstrates the equation of motion pertaining to a damped vibrational force. In general, it is segmented into external and internal forces. On the left-hand side of the equation are the internal forces, while the right-hand side of the equation includes external forces. External forces brought about by engine operations, tires etc. have an effect on the simulation results. However, this was not premeditated in this research work.

Hence, the equation of motion was transformed into a damped free vibration, obtained below:

$$m\ddot{x} + d\dot{x} + kx = 0 \tag{6}$$

The displacement x is attained as:

$$x = \frac{-m\ddot{x} - d\dot{x}}{k} \tag{7}$$

Shearing forces generate shearing deformation. Any object that is susceptible to shear has its shape or form altered but does not affect the length. The alteration in the angle of that object at some point in time is referred to as the shear strain. If the shear strain γ is combined with the tension in the spring, the equation can then be illustrated as:

$$\gamma = \frac{x}{D_0} \tag{8}$$

where D_0 is the initial unloaded diameter. Substituting Eq. (7) into Eq. (8), the shear strain γ is:

$$\gamma = \frac{-m\ddot{x} - d\dot{x}}{kD_0} \tag{9}$$

Differentiation of velocity can help to determine acceleration. Primarily, velocity is obtained based on mechanical means for a short period of time due to limitation associated with the transducers. However, if a stiff body accelerates at a detectable time intervals, velocity could be produced by connecting time-dependent acceleration. Therefore, the equation explains the shear strain γ:

$$\gamma = \frac{-m\ddot{x} - d\int \ddot{x}}{kD_0} \tag{10}$$

Since the current study did not gather acceleration signals, the actual strain signals were employed in order to observe vibration responses. The acceleration $\ddot{x}$ was produced by:

$$\ddot{x} = -\frac{-d\dot{x} - kx}{m} \tag{11}$$

The velocity $\dot{x}$ can be determined from the known displacement x by the differentiation of the time-dependent movement. Expanding Eq. (11), then:

$$\ddot{x} = -\frac{-d\left(\dfrac{\partial x}{\partial t}\right) - kx}{m} \tag{12}$$

where t is the time. Substituting Eq. (8) into Eq. (12), the acceleration $\ddot{x}$ results:

$$\ddot{x} = -\frac{-d\left(\dfrac{\partial(\gamma D_0)}{\partial t}\right) - k\gamma D_0}{m} \tag{13}$$

Some useful tools used in solving problems in these areas are computer-based modelling and virtual experimentation. A modelling technique that was derived from the adjustment of the object and the equations for dynamic systems [50] was used to produce a strain signal that had the same function as that of the real strain signal. The illustrative diagram generated was derived from Eq. (10) as depicted in combiTimeTable of Figure 3, which proposed the input of a variable dataset that linked to the position thereby deciding the motion of the coil spring system. World depicts the coordinate system, and prismatic depicts the degree of freedom. The spring damper was put forward as input for the damping coefficient as well as the spring stiffness, and for the body, the mass was recommended. Absolute sensor altered the variable datasets into accelerations. In the controller, obtaining of the strains was done by considering the input pertaining to the real expression, which is also the initially expunged length related to the coil spring. Finally, a simulated strain signal generated by the acceleration is offered in the gain.
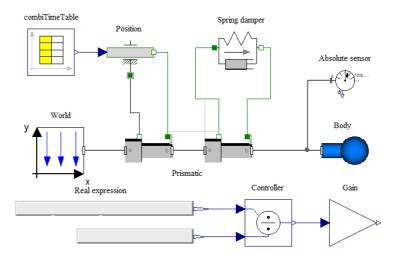

Figure 3. Diagram for strain signal simulation.

For validating the strain signals, a comparison was carried out between the simulated and the actual strain signals utilising fatigue tests. The variable amplitude loading (VAL) fatigue tests were carried out to certify the fatigue lives of the strain signals. Any hypothesis cannot determine the fatigue lives of complex loadings [29-30]. The strain signals were changed into stress with the aid of the Ramberg-Osgood equation [51] outlined below:

$$\varepsilon = \frac{\sigma}{E} + K'\left(\frac{\sigma}{E}\right)^{n'} \tag{14}$$

where ε is the strain, σ is the stress, E is the material modulus of elasticity, K' is the cyclic strength coefficient and n' is the cyclic strain hardening exponent. Consequently, transformation of the stress was done into loads, which were employed as an input value pertaining to the fatigue testing device along with the expression presented below:

$$\sigma = \frac{P}{A_0} \tag{15}$$

where A_0 is the initial unloaded cross-sectional area. Figure 4 shows all the generated fatigue testing samples per ASTM E606-92 [52]. This included description of the ranges of samples, the geometry, and the suitable grips employed in fatigue testing device. Production of the samples was done with the help of computer numerical controls and as well as grinding machines. Post this; automatic refining [43] was done for these in order to ensure eliminating the machine marks gradated during testing. The entire tests were conducted by maintaining a room temperature of 20 ºC [52]. A 100 Hz frequency value was employed to carry out the reversed VAL fatigue tests. Figure 5 depicts the general procedure of this work.
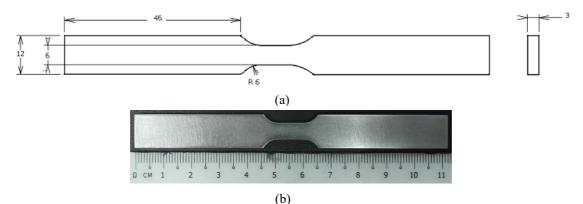

(a)

(b)

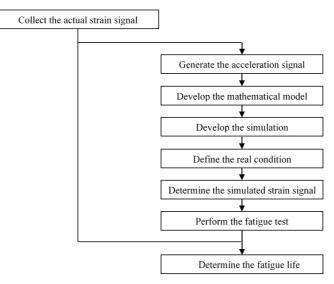**Figure 4.** Fatigue test sample (a) geometry and dimensions in millimetres, (b) photograph.

Figure 5. Process flow of the study.

RESULTS AND DISCUSSION

When in some areas, the stress gets intensified, then smaller elements are recommended for such regions. Hence, if the value of the mesh is high, it means merely a desire for meshes with acceptable features. Sadly, with a rise in the

number of elements, the required computational time also gets extended. Thus, it is of utmost importance to restrict the number of elements [53]. A mesh type that has eight sides (tetrahedral) is mainly believed to be acceptable and is presumed to be a high-quality mesh that can be used for boundary representation of the solid model. It also used to generate detail result. Meshing was done by using a set of nodes to separate the geometry of the model components, thereby producing smaller pieces called elements. To the entire minor portions, applying of the von Mises yield criterion was done. Thus, by accounting for the global seeds, 3,710 elements were generated by making use of 10,999 nodes.

The colour contour pertaining to the stress concentration for the coil spring is shown in Figure 6. In the figure, the areas having the highest amount of stress concentration is shown in red, which is followed by regions in orange, yellow, green and blue, respectively. A maximal von Mises stress value of 1.199 MPa is demonstrated by the areas in red, which occurred at node 3,463. Based on Table 1, it can be inferred that the maximum stress was exceptionally low versus the 1.48 GPa yield strength, which suggests that the force did not result in any particular deficiency for the coil spring. The inner area is smaller when compared with the outside area, causing the critical area to occur on the inside of the coil spring. The critical area also occurs at the border between active and inactive coils [27, 29-30, 54].
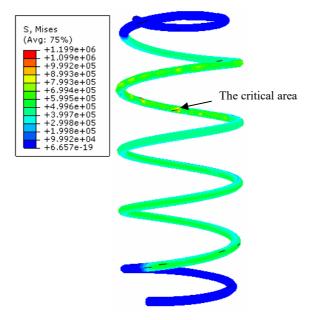

Figure 6. Stress distributions of the coil spring

The strain signals received by the strain gauge was examined to be a VAL due to the various amplitudes that were tested by the component. 60-second strain signals were recorded as described in Figure 7. The rural road provided a higher amplitude range since the road was a rough surface with holes and bumps. Furthermore, the urban and rural strain signals are called S1 and S2, respectively.
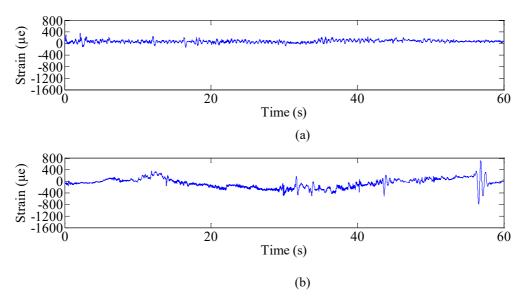

(a)

(b)

Figure 7. Time histories of the actual strain signals: (a) S1-urban, (b) S2-rural.

Figure 8 is an illustration of the trend of acceleration obtained on both the urban and rural roads. The strains with larger amplitudes resulted in larger accelerations. These were following the strain signals depicted in Figure 7. The acceleration signal gotten from the country roads generated larger amplitudes due to the strain signal obtained from an uneven surface. This revealed that the road surface depicts more significant vibrational energy as a result of the larger strain amplitude.
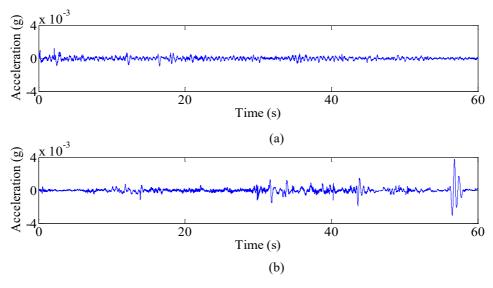

(a)

(b)

Figure 8. Time histories of the acceleration signals: (a) urban, (b) rural.

Additionally, the acceleration signals were computed for the multi-body dynamic (MBD) simulation to produce other strain signals. The acceleration model as per Eq. (10) was employed to produce the strain signals, as shown in Figure 9. To effectively operate the MBD simulation, the mass, the stiffness of the spring, the damping coefficient and the initial diameter must be observed. It was shown to show high consistency, which depicts higher probability of correlation pertaining to the two strain signals. However, the simulated strain signals were found to change the amplitude range. This was caused by the employed equation of motion in order to produce the uncomplicated model without accounting for the external forces.

According to the results obtained from the fatigue testing, the actual strain signal of the urban road (S1) requires not less than 412 reversals of blocks until there was a decline in the time duration which was over 34.3 hours. The increment of the time by 0.7 % or by 34.6 hours was determined using the simulated urban strain signal (S3) with 415 reversals of blocks. The rural roads revealed the same circumstance. The time required was 11.4 hours to carry out the fatigue test pertaining to the actual strain signal on the rural road (S2) along with 137 reversals of blocks. A 1.5 % increase in the fatigue testing time was seen when the reversals of blocks was increased to 139 for the simulated strain signal (S4).
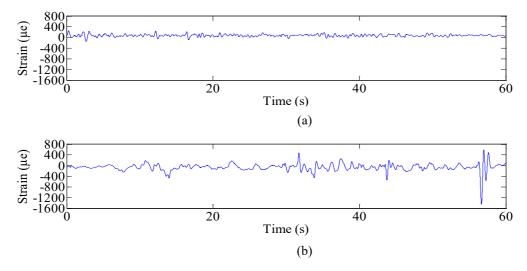

(a)

(b)

Figure 9. Time histories of the simulated strain signals; (a) S3-urban, (b) S4-rural.

The fatigue testing results showed that the simulated fatigue life was almost directly proportional to that of real fatigue life, while the manufactured MBD model was identical with an excellent result. Through this simulation, a strain signal can be created where integrity and fatigue failure of the developed strain signals can adequately be identified, thereby, saving the cost associated with operation and maintenance. Finally, this developed MBD simulation is suggested to assist the automotive industries involved with fatigue-based strain signal acquisitions.

CONCLUSION

In this study, a technique was proposed to generate strain signals based on a simulation which considered the acceleration signals leading to fatigue failure. This study was started by identifying the stress distributions at a coil spring. The stress distributions eased to identify the critical point at the component. After the critical point has been analysed, the strain signal measurement that is obtained during the vehicle operation can then be performed. The actual strain signals were utilised for the inputs in the MBD simulation yielding the simulated strain signals. The fatigue life of the actual and simulated strain signals were examined providing the values of 412, 415, 137 and 139 reversals of blocks, respectively, for the actual urban, simulated urban, actual rural, and simulated rural strain signals. According to fatigue testing results, the actual and simulated strain signals had an equivalent fatigue life. The results were certified as accurate with the deviations of fatigue life was lower than 1.5 %. This acts as a guide for discovering new methods for measuring the strain signals. The results from this research could increase the connection between the virtual and the actual world of durability testing. Theoretical estimation of the road surface profile was employed for the complete MBD simulation, which demonstrated dissimilarity on comparison with the real situation. Thus, generation of a geometrical model concerning the road surface profiles is important in order to yield an outstanding effect regarding the strain signal production. In recent work, the geometrical model could be integrated with the MBD model. Consequently, the procurement of acceleration and strain signals are no longer required.

ACKNOWLEDGEMENT

REFERENCES

[1]   Ye XW, Su YH, Han JP. A state-of-the-art review on fatigue life assessment of steel bridges. Mathematical Problems in Engineering 2014; 1-13.

[2]   Zakaria KA, Abdullah S, Ghazali MJ. A review of the loading sequence effects on the fatigue life behaviour of metallic materials. Journal of Engineering Science and Technology Review 2016; 9: 189-200.

[3]   Bishop NWM, Sherratt F. Finite element based fatigue calculations. London: NAFENS; 2000.

[4]   Kopas P, Saga M, Baniari V, Vasko M, Handrik M. A plastic strain and stress analysis of bending and torsion fatigue specimens in the low-cycle fatigue region using the finite element methods. Procedia Engineering 2017; 177: 526-531.

[5]   Khan SMA, Benyahia F, Bouiadjra BB, Albedah A. Analysis and repair of crack growth emanating from V-notch under stepped variable fatigue loading. Procedia Engineering 2014; 74: 151-156.

[6]   Anes V, Reis L, Freitas M. Multiaxial fatigue damage accumulation under variable amplitude loading conditions. Procedia Engineering 2015; 101: 117-125.

[7]   Vormwald M. Multi-challenge aspects in fatigue due to the combined occurrence of multiaxiality, variable amplitude loading, and size effects. Frattura ed Integrità Strutturale 2015; 33: 253-261.

[8]   Silva AL, Varanis M, Mereles AG, Oliveira C, Balthazar JM. A study of strain and deformation measurement using the Arduino microcontroller and strain gauges devices. Revista Brasileira de Ensino de Física 2019; 41.

[9]   Lener G, Lang R, Ladinek M, Timmers R. A numerical method for determining the fatigue strength of welded joints with a significant improvement in accuracy. Procedia Engineering 2018; 213: 359-373.

[10]   Motra HB, Hildebrand J, Dimmig-Osburg A. Assessment of strain measurement techniques to characterise mechanical properties of structural steel. Engineering Science and Technology, an International Journal 2014; 17: 260-269.

[11]   Stoney R, Pullen T, Aldwell B, Gierlings S, Brockmann M, Geraghty D, Veselovac D, Klocke F, Donnell GEO. Observations of surface acoustic wave strain and resistive strain measurements on broaching tools for process monitoring. Procedia CIRP 2014; 14: 66-71.

[12]   Oh C-S. Application of wavelet transform in fatigue history editing. International Journal of Fatigue 2001; 23: 241-250.

[13]   Haiba M, Barton D, Brooks P, Levesley M. The development of an optimisation algorithm based on fatigue life. International Journal of Fatigue 2003; 25: 299-310.

[14]   Ilic S. Methodology of evaluation of in-service load applied to the output shafts of automatic transmissions. Ph.D. Thesis. The University of New South Wales; 2006.

[15]   Abdullah S, Choi JC, Giacomin JA, Yates JR. Bump extraction algorithm for variable amplitude fatigue loading. International Journal of Fatigue 2006; 28: 675-691.

[16]   Baek SH, Cho SS, Joo WS. Fatigue life prediction based on the rainflow cycle counting method for the end beam of a freight car bogie. International Journal of Automotive Technology 2008; 9: 95-101.

[17]   Alaoui AEM, Thevenet D, Zeghloul A. Short surface fatigue cracks growth under constant and variable amplitude loading. Engineering Fracture Mechanics 2009; 76: 2359-2370.

[18]   He B-Y, Wang S-X, Gao F. Failure analysis of an automobile damper spring tower. Engineering Failure Analysis 2010; 17: 498-505.

[19] Oskoueian A, Nuawi MZ. Internal combustion engine monitoring using strain gauge and analysing with I-Kaz. IERI Procedia 2012; 1: 192-198.

[20] Aygül M, Al-Emrani M, Urushadze S. Modelling and fatigue life assessment of orthotropic bridge deck details using FEM. International Journal of Fatigue 2012; 40: 129-142.

[21] Lin C-H, Lin K-C, Tsai K-C, Jhuang S-J, Lin M-L, Chen P-C, Wang K-J, Lin S-L, Chen J-C. Full-scale fatigue tests of a cable-to-orthotropic bridge deck connection. Journal of Constructional Steel Research 2012; 70: 264-272.

[22] Xia HW, Ni YQ, Wong KY, Ko JM. Reliability-based condition assessment of in-service bridges using mixture distribution models. Computers and Structures 2012; 106-107: 204-213.

[23] Ye XW, Ni YQ, Wong KY, Ko JM. A statistical analysis of stress spectra for fatigue life assessment of steel bridges with structural health monitoring data. Engineering Structures 2012; 45: 166-176.

[24] Ye XW, Ni YQ, Ko JM. Experimental evaluation of stress concentration factor of welded steel bridge T-joints. Journal of Constructional Steel Research 2012; 70: 78-85.

[25] Kihm F, Delaux D. Vibration fatigue and simulation of damage on shaker table tests: the influence of clipping the random drive signal. Procedia Engineering 2013; 66: 549-564.

[26] Lei L, Decheng X, Min Y, Fei X, Jiawang J, Guodong Z, Wensheng Z. Strain test and stress intensity assessment of a CPR1000 nuclear power plant pressuriser during pre-delivery hydrostatic test. Case Studies in Structural Engineering 2014; 2: 41-51.

[27] Putra TE, Abdullah S, Schramm D, Nuawi MZ, Bruckmann T. Generating strain signals under consideration of road surface profiles. Mechanical Systems and Signal Processing 2015; 60-61: 485-497.

[28] He J, Zhou Y, Guan X, Zhang W, Wang Y, Zhang W. An integrated health monitoring method for structural fatigue life evaluation using limited sensor data. Materials 2016; 9.

[29] Putra TE, Abdullah S, Schramm D, Nuawi MZ, Bruckmann T. Reducing cyclic testing time for components of automotive suspension system utilising the wavelet transform and the Fuzzy C-Means. Mechanical Systems and Signal Processing 2017; 90: 1-14.

[30] Putra TE, Abdullah S, Schramm D, Nuawi MZ, Bruckmann T. The need to generate realistic strain signals at an automotive coil spring for durability simulation leading to fatigue life assessment. Mechanical Systems and Signal Processing 2017; 94: 432-447.

[31] Zhang Z, Zhang Y, Kos A, Umek A. Strain gage sensor based golfer identification using machine learning algorithms. Procedia Computer Science 2018; 129: 135-140.

[32] Nasir NNM, Abdullah S, Singh SSK, Haris SM. Extreme condition strain signal reliability assessment using empirical mode decomposition. In: Proceedings of Mechanical Engineering Research Day, pp. 23-24; 2018.

[33] Rahim AAA, Abdullah S, Singh SSK, Nuawi MZ. Discrete wavelet transform method for fatigue analysis on car suspension system. In: Proceedings of Mechanical Engineering Research Day, pp. 22-26; 2018.

[34] Ren P, Zhou Z. Strain response estimation for the fatigue monitoring of an offshore truss structure. Pacific Science Review 2014; 16: 29-35.

[35] Ge J, Sun Y, Xu J, Yang Z, Liang J. Fatigue life prediction of metal structures subjected to combined thermal-acoustic loadings using a new critical plane model. International Journal of Fatigue 2017; 96: 89-101.

[36] Kharrat M, Ramasso E, Placet V, Boubakar L. Acoustic emission in composite materials under fatigue tests: effect of signal-denoising input parameters on the hits detection and data clustering. In: 31st Conference of the European Working Group on Acoustic Emission (EWGAE); 2014.

[37] Zhu Y, Jiang W, Kong X, Zheng Z, Hu H. An accurate integral method for vibration signal based on feature information extraction. Shock and Vibration 2015.

[38] Upadhyay R, Padhy PK, Kankar PK. EEG artifact removal and noise suppression by Discrete Orthonormal S-Transform denoising. Computers and Electrical Engineering 2016; 53: 125-142.

[39] Amrutha N, Arul VH. A review on noises in EMG signal and its removal. International Journal of Scientific and Research Publications 2017; 7: 23-27.

[40] Jiang F, Zhu Z, Li W, Zhou G, Xia S. Noise reduction in feature level and its application in rolling element bearing fault diagnosis. Advances in Mechanical Engineering 2018; 10: 1-10.

[41] nCode. GlyphWorks. Sheffield: nCode International, Ltd.; 2018.

[42] ASTM E1237-93. Standard guide for installing bonded resistance strain gages. West Conshohocken: ASTM International; 2014.

[43] ASTM E112. Standard test methods for determining average grain size. West Conshohocken: ASTM International; 2010.

[44] Ning X, Zhao C, Shen J. Dynamic analysis of car suspension using ADAMS/car for development of a software interface for optimisation. Procedia Engineering 2011; 16: 333-341.

[45] Peters S, Lanza G, Ni J, Xiaoning J, Pei-Yun Y, Colledani M. Automotive manufacturing technologies - an international viewpoint. Manufacturing Review 2014; 1.

[46] Roman L, Florea A, Cofaru II. Software application for assessment the reliability of suspension system at OPEL cars and of road profiles. Fascicle of Management and Technological Engineering 2014; 1: 289-294.

[47] Tandel A, Deshpande AR, Deshmukh SP, Jagtap KR. Modeling, analysis and PID controller implementation on double wishbone suspension using SimMechanics and Simulink. Procedia Engineering 2014; 97: 1274-1281.

[48]   Ott RJ. Understanding pyrotechnic shock dynamics and response attenuation over distance. Ph.D. Thesis. Utah State University; 2016.

[49]   Zhang H, Zhang X, Wang J. Robust gain-scheduling energy-to-peak control of vehicle lateral dynamics stabilisation. Vehicle System Dynamics 2014; 52: 309-340.

[50]   Elmqvist H. A structured model language for large continuous systems. Ph.D. Thesis. Lund Institute of Technology; 1978.

[51]   Ramberg W, Osgood WR. Description of stress-strain curves by three parameters. National Advisory Committee for Aeronautics 1943.

[52]   ASTM E606-92. Standard practice for strain-controlled fatigue testing. West Conshohocken: ASTM International; 2004.

[53]   Ramesh S. Implementation of space-time finite element formulation in elastodynamics. M.Sc. Thesis. Rose-Hulman Institute of Technology; 2016.

[54]   Zhu Y, Wang Y, Huang Y. Failure analysis of a helical compression spring for a heavy vehicle's suspension system. Case Studies in Engineering Failure Analysis 2014; 2: 169-173.